© 1965 IEEE. Personal use of this material is permitted. However, permission to reprint/republish this material for advertising or promotional purposes or for creating new collective works for resale or redistribution to servers or lists, or to reuse any copyrighted component of this work in other works must be obtained from the IEEE.

SOME NEW RADIO FREQUENCY ACCELERATING STRUCTURES*

S. Giordano
Brookhaven National Laboratory
Upton, L.I., N.Y.

Introduction

This paper deals primarily with a multiply periodic radiofrequency structure operating as a standing wave $\pi/2$-mode accelerator. The advantages of this structure are a high shunt impedance, and a greater mode separation around the operating mode. A comparison is made between the above-mentioned multiply periodic structure, and symmetrical structures such as the cloverleaf, slotted-iris, and disc-loaded waveguide.

Choice of Structure

A number of laboratories have been considering the design of high energy proton linacs with output energies of 500 to 1000 MeV. Once the operating parameters of the machine have been defined, such as final energy, beam intensity, output emittance, etc., the design of all components must be carefully considered to achieve reliable operation at a minimum cost. One of the major components that must be considered for both reliability and cost, is the radiofrequency accelerating structure. There is no single criterion that can be used to define a good structure. Any structure selected must be, by necessity, a compromise of the following three considerations: (1) relatively high shunt impedance, to keep the total radiofrequency power within reasonable limits, (2) reduced sensitivity to tank detuning and beam loading effects, to achieve stable operation, (3) operation of the structure as an integrated part of a complex machine.

This report deals primarily with structures above the energy range of 200 MeV. To date, most of the structures that have been considered are the symmetric periodically loaded, such as cloverleaf, slotted-iris, and iris-loaded waveguide, operating as a π-mode standing wave accelerator. Extensive investigation of the above-mentioned structures, have been carried out at various laboratories using both equivalent circuit analysis and model measurements. The properties of these structures have previously been reported.[1-6]

It is possible to operate any of the three-mentioned structures in any mode between 0 and π. Figure 1a shows a typical dispersion curve for a backward wave structure. (It should be pointed out that for the purpose of this discussion we will consider backward wave structures, but the same conclusions apply to forward wave structures.) For a fixed β, Figures 1b and 1c show the variation of R_{sh} (shunt impedance), and v_g (group velocity = $d\omega/d\beta$, where ω = angular frequency and $\beta = 2\pi/\lambda g$, where λg = guide wavelength). We see from Figures 1b and 1c that the highest R_{sh} occurs at the π mode, where the group velocity is zero.

To reduce beam loading and tank detuning effects it is desirable to do either of the following:

1. Make $|d\omega/d\beta|$ as large as possible. This corresponds to working in the middle of a passband. In Fig. 1 we see that this occurs at the $\pi/2$ mode where the shunt impedance is considerably lower than the π mode.

2. Make $|d^2\omega/d\beta^2|$ as large as possible. This corresponds to working at the edge of a passband (such as the π mode) and making the bandwidth as large as possible. (B.W. = bandwidth = $|2(\omega_o - \omega_\pi)/\omega_o + \omega_\pi|$, where ω_o = angular frequency of the π mode.) It should be pointed out that either of the above two steps results in a greater mode separation around the operating mode.

One of the main reasons for the reduction of R_{sh} in the $\pi/2$ mode as compared to the π mode is due to the difference of the variation of the axial electric field. In Figures 2a and 2b, we have two structures which have the same β, operating in the π and $\pi/2$ mode respectively, showing the variation of $|\bar{E}|$. ($\bar{E}$ = peak axial electric field and is a function of both z and t.)

For a synchronous particle, the shunt impedance is defined as

$$R_{sh} = \frac{\left[\int_0^L \bar{E} \cdot d\bar{z} \right]^2}{\int_0^L P \, dz} ,$$

(this includes the transit time factor but not the synchronous phase angle), where P is the power loss per unit length as a function of z, and the limits of integration are taken from 0 to L, which represents a periodic length of the electric field variation as shown in Fig. 2. Various measurements have shown that $R_{sh}(\pi/2)$ is between 1/3 and 1/2 of $R_{sh}(\pi)$, [where $R_{sh}(\pi)$ and $R_{sh}(\pi/2)$ are the shunt impedance of the π mode and $\pi/2$ mode respectively] for a symmetric periodically loaded structure. In the above equation for R_{sh}, if we write $\bar{E} = Ef(z,t)$, where E is simply a magnitude, then

$$R_{sh} = \frac{E^2 \left[\int_0^L f(z,t) dz \right]^2}{\int_0^L P \, dz} .$$

* Work done under the auspices of the U.S. AEC.

Since E^2 is proportional to the stored energy, therefore

$$Q \propto \frac{E^2}{\int_0^L P\,dz} ,$$

and we may now write

$$R_{sh} = KQ\left[\int_0^L f(z,t)dz\right]^2 .$$

Comparing some of the measured values of R_{sh} and Q for the $\pi/2$ and π mode in the above equation, we find that the value of

$$\int_0^L f(z,t)dz$$

for the π mode is larger than the same integral evaluated for the $\pi/2$ mode. The

$$\int_0^L f(z,t)dz$$

can now be related to the transit time factor, to show that the transit time factor for the π mode is greater than the $\pi/2$ mode.

Multiply Periodic Structure

In Fig. 3 we have a new structure by alternating the periodicity of the cells. By making $L_4 < L_3$, and operating in the $\pi/2$ mode, there is a considerable improvement in the transit time factor as compared to the conventional symmetric $\pi/2$ mode. This structure is referred to as being multiply periodic.

If only the cell lengths are alternated and no nose cones are used, the original passband is split into an upper and lower passband, with a stopband between the two passbands as shown in Fig. 4a. Figures 4b and 4c show the group velocity and R_{sh} for the above-mentioned structure.

It is seen from Figures 4b and 4c that, although the shunt impedance of the $\pi/2$ mode has been improved, the group velocity v_g is zero at the $\pi/2$ mode. It is now possible to detune alternate cells (either by perturbation tuners or by adding nose cones as shown in Fig. 3) to join the upper and lower sidebands together and eliminate the stopband. The above results in a dispersion curve as shown in Fig. 4d and the resulting group velocity and shunt impedance curve shown in Figures 4e and 4f.

It was found experimentally that in the $\pi/2$ mode, the tuning characteristics of the multiply periodic structure shown in Fig. 3 have some interesting properties. A perturbation tuner, in the form of a copper rod passing through a hole in the side wall, was placed in each cell. By adjusting the tuners in the small cells only, two interesting effects were observed: (1) the resonant frequency of the $\pi/2$ mode did not change, which meant that for the $\pi/2$ mode there is no stored energy in the small cell, (2) the frequency of all other modes, except the $\pi/2$, were affected by these tuners, which means that it is possible to change the shape of the dispersion curve without affecting the frequency of the $\pi/2$ mode.

Other experimental measurements were made with a demountable cavity using sheet metal irises. The model used H-field coupling, resulting in a backward wave structure. Typically, the irises used are shown in Fig. 5a. Tuning of alternate cells was accomplished by adjusting the nose cone length. (Nose cone lengths can also be adjusted to optimize shunt impedance.) Figure 5b shows a typical structure.

Measurements of shunt impedance were made on three different models listed below:

β	Small Cell Length	Large Cell Length	Drift Tube Length	R_{sh}
.5	.5"	3"	.25"	16 MΩ/m
.6	.25"	4"	.375"	22 MΩ/m
.8	1.5"	4"	.25"	28 MΩ/m

Each of the above models had a 2.125" bore hole. The measured values of shunt impedance compare favorably with cloverleaf, slotted iris, and iris-loaded structures operating in the π mode. It was also found that the alternating cell structures were at least ten times less sensitive to tank detuning errors than a conventional π mode structure.

At β = .5 the cavities were tuned so that we had a continuous dispersion curve as shown in Fig. 4d. At β = .8 the cavities were tuned so that a stopband of approximately 7 Mc existed between the upper and lower sideband as shown in Fig. 6. The upper bandpass contains the $\pi/2$ mode of interest, while the lower bandpass has a redundant $\pi/2$ mode. In Fig. 6 we see that the dispersion curve for the upper bandpass is very asymmetrical, resulting in the desirable condition of a large $|d^2\omega/d\beta^2|$ at the $\pi/2$ mode.

It should be pointed out that in Fig. 6 the dispersion curve is for the structure shown in Fig. 5. If the boundary conditions are changed to those shown in Fig. 7a, then the resulting dispersion curve is that as shown in Fig. 7b, where the $\pi/2$ mode is contained in the lower passband, but not in the upper passband. This $\pi/2$ mode in the lower passband has a very low R_{sh}.

Work is presently progressing on some new models. Physically longer models are required to get more definite results of tank tuning and beam loading effects.

Future Programs

The problems of tank detuning and beam loading effects are directly related to the spacing of the modes adjacent to the operating mode, and also to L_T^2 (when L_T is the total length of a single tank). Presently, for a π-mode structure, tank lengths of approximately 3 or 4 meters have been considered a reasonable compromise. For a $\pi/2$-mode structure it may be possible to increase the length of a single tank to 30 meters. There are many advantages of having long tanks. For example, in a 500-MeV linac, there may be as many as 50 tanks, each 3 meters long, with a separate power amplifier driving each tank. If just one of these power amplifiers fails, the linac ceases operation. If instead, we had five tanks, each 30 meters long, each tank would have 10 amplifier driving ports distributed along its length. The failure of any of these amplifiers can easily be compensated for by slightly increasing the power output of the remaining nine amplifiers, and the linac can continue operating. The feasibility of this scheme is presently being investigated.

A new structure presently being investigated is shown in Fig. 8a, with its associated dispersion curve shown in Fig. 8b. Figure 8a also shows the field configuration for the $\pi/2$ mode. As shown in Fig. 8a, the structure has five irises, but it may also be possible to replace the second and fourth iris by a short drift tube supported by a stem. It will be necessary to adjust the electric field loading on the irises and drift tube to achieve the dispersion curve as shown in Fig. 8b. Some very preliminary measurements indicate that the structure may have some interesting possibilities. It should be pointed out that in this structures the π mode is missing.

I would like to thank Dr. J.P. Blewett and Dr. T. Nishikawa for their useful discussions.

References

1. E.A. Knapp, "Accelerating Structure Research at Los Alamos", Minutes of the Conference on Proton Linear Accelerators at Yale University, October 21-25, 1963, p. 131.

2. S. Giordano, "Measurements on Iris-Loaded Waveguides", ibid., p. 153.

3. D.E. Nagle, E.A. Knapp, "Steady State Behavior of a Ring or a Chain of Coupled Circuits", ibid., p. 171.

4. R.L. Gluckstern, "Effects of Errors in Repetitive Structures", ibid., p. 190.

5. S. Giordano, "Model Measurements and Correction of Beam Loading Effects in Proton Linacs", Minutes 1964 MURA Conference on Proton Linear Accelerators, p. 252.

6. S. Giordano, "Characteristics of Slotted Irises", ibid., p. 60.

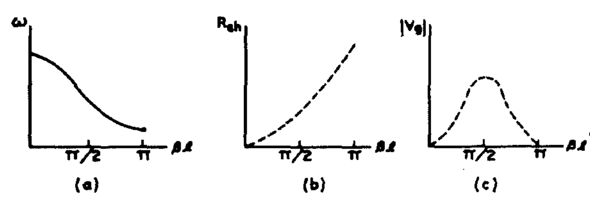

Fig 1. Symmetric periodically loaded forward wave structure.

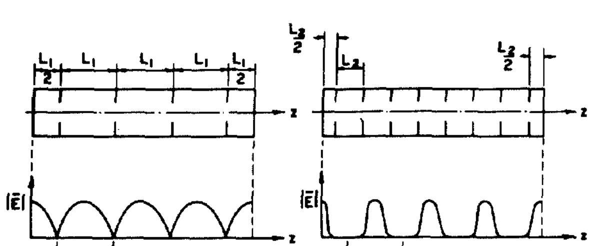

Fig. 2. (a) Symmetric π mode.
(b) Symmetric $\pi/2$ mode.

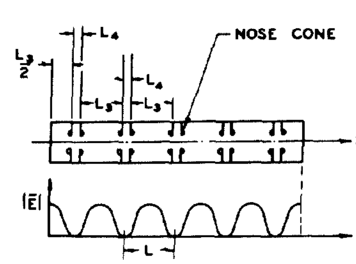

Fig. 3. Alternating periodic $\pi/2$ mode.

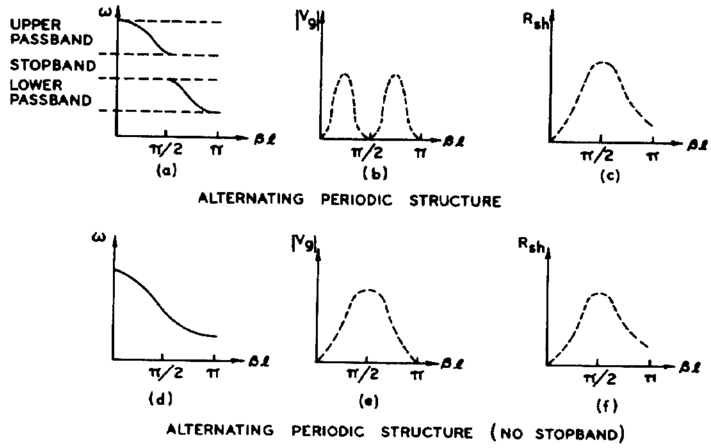

Fig. 4. Alternating periodic structure.

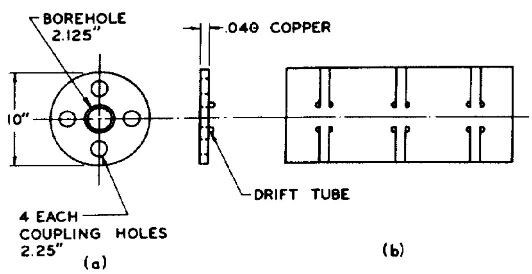

Fig. 5. Alternating periodic structure.

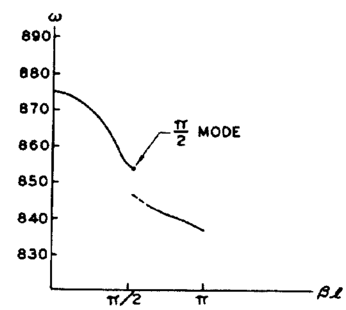

Fig. 6. Dispersion curve alternating periodic structure.

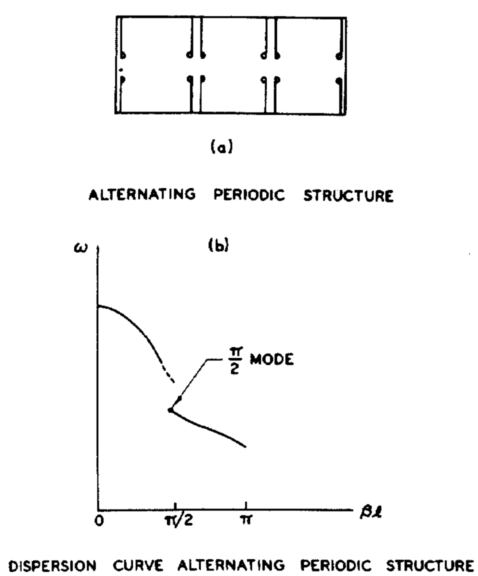

Fig. 7.

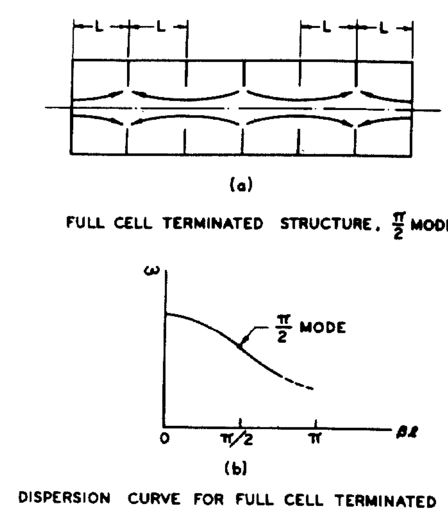

Fig. 8.